Mechanical Systems and Signal Processing (1998) **12**(1), 47–64

REGULARISATION METHODS FOR FINITE ELEMENT MODEL UPDATING

H. Ahmadian

Department of Mechanical Engineering, Iran University of Science and Technology, Narmak, Tehran, Iran

J. E. Mottershead

Department of Mechanical Engineering, The University of Liverpool, U.K.

AND

M. I. Friswell

Department of Mechanical Engineering, University of Wales Swansea, U.K.

(Received September 1996, *accepted after revisions April* 1997)

This paper addresses the problem of selecting a side constraint and determining the regularisation parameter in model updating. The weight to be attached to the constraint is determined by the regularisation parameter. Methods based on singular value decomposition, cross-validation, and L-curves are considered, and results obtained by applying these methods to a numerical example provide the basis for a comparative study. It is found that the method of cross-validation can be used reliably to truncate the small generalised singular values which contain the measurement noise. The L-curves approach is similarly robust in locating the regularisation parameter, and this is demonstrated in a physical experiment. It is shown that careful selection of the side constraint can lead to updated parameters with physical understanding.

1. INTRODUCTION

Noise contamination in test data is a problem central to finite element model updating [1, 2]. The purpose of this article is to demonstrate how regularisation methods can be used for the treatment of ill-conditioned, noisy systems of equations such as those that arise in the correction of finite element models by using vibration measurements.

The regularisation problem centres around the equation,

$$\boldsymbol{A}\boldsymbol{\theta} = \boldsymbol{b}, \tag{1}$$

where $\boldsymbol{A} \in \mathscr{R}^{n \times m}$, $\boldsymbol{b} \in \mathscr{R}^{n \times 1}$, $\boldsymbol{\theta} \in \mathscr{R}^{m \times 1}$, $n > m$, and the parameters $\boldsymbol{\theta}$ are required. Initially, consider the case when $\boldsymbol{b}$ is contaminated with additive random noise, $\boldsymbol{\varepsilon}$, having zero mean and with mutually independent entries (the case of noise being present in the matrix $\boldsymbol{A}$ will be discussed later). It is well known that the least-squares solution, $\boldsymbol{\theta}_{LS}$, is unique and unbiased provided that $\text{rank}(\boldsymbol{A}) = m$. When $\boldsymbol{A}$ is close to being rank deficient then a small $\boldsymbol{\varepsilon}$ may lead to a large deviation in $\boldsymbol{\theta}$ from its exact value and the solution is said to be unstable and equation (1) is ill-conditioned.

0888–3270/98/010047 + 18 $25.00/0/pg960133

A different problem occurs when $m > n$ so that equation (1) is undetermined and there are an infinite number of solutions. The Moore–Penrose pseudo-inverse in the form,

$$\boldsymbol{\theta}_{LS} = \boldsymbol{A}^T(\boldsymbol{A}\boldsymbol{A}^T)^{-1}\boldsymbol{b}, \tag{2}$$

provides the solution of minimum norm, as does singular value decomposition (SVD). For the case when $\text{rank}(\boldsymbol{A}) = r < \min\{m, n\}$, Golub and Van-Loan [3] showed that the SVD will result again in the minimum norm solution. This is a form of regularisation which has been applied widely in the model updating community [4–6]. Rothwell and Drachman [7] developed a method that resulted in a diagonal matrix with terms $(\sigma_i + \lambda^2/\sigma_i)$, where the conditioning is controlled by adjusting λ, and σ_i denotes the ith singular value.

Natke [8, 9] advocated the application of regularisation techniques in model updating and Fregolent *et al*. [10] considered a variety of methods for determining the regularisation parameter, λ, in the equation-error problem. Link [11] weighted the parameters by a diagonal matrix related to the reciprocals of the sensitivity terms, which had the effect of constraining those parameters with small sensitivities. Prells [12] used in a weighting matrix based on data sensitivities calculated from a Monte-Carlo-like method. The present study considers the ill-conditioned system of n equations in m parameters ($n \geqslant m$). An important objective is to provide a physical interpretation of regularised results, which is demonstrated in numerical and physical examples.

2. STATEMENT OF THE PROBLEM

The classical Tikhonov/Phillips regularisation problem can be described as follows: Determine the stable solution, $\boldsymbol{\theta}$, of equation (1) which approaches the true solution $\boldsymbol{\theta}_{EX}$,

$$\boldsymbol{A}\boldsymbol{\theta}_{EX} = \boldsymbol{b} - \boldsymbol{\varepsilon}, \tag{3}$$

as the noise (present in $\boldsymbol{b}$) becomes vanishingly small,

$$\boldsymbol{\theta} \to \boldsymbol{\theta}_{EX}, \qquad \boldsymbol{\varepsilon} \to \boldsymbol{0}. \tag{4, 5}$$

In Tikhonov's method [13] the approximate solution, $\boldsymbol{\theta}(\lambda)$, is defined as the unique minimiser of the quadratic cost function,

$$\|\boldsymbol{A}\boldsymbol{\theta} - \boldsymbol{b}\|_2^2 + \lambda\|\boldsymbol{C}\boldsymbol{\theta} - \boldsymbol{d}\|_2^2, \tag{6}$$

where $\boldsymbol{C} \in \mathscr{R}^{p \times m}$, $p \leqslant m$, is chosen so that

$$\text{rank}\begin{bmatrix}\boldsymbol{A}\\ \boldsymbol{C}\end{bmatrix} = m, \tag{7}$$

which is an expression of Morozov's complementation condition [14], and $\lambda > 0$ is the regularisation parameter (some authors use λ^2 in place of λ). The basic idea is to minimise the cost (6) by searching for a solution $\boldsymbol{\theta}(\lambda)$ which at the same time produces a small residual $\|\boldsymbol{A}\boldsymbol{\theta}(\lambda) - \boldsymbol{b}\|_2^2$ and a moderate value of the side constraint $\|\boldsymbol{C}\boldsymbol{\theta}(\lambda) - \boldsymbol{d}\|_2^2$. The way in which these two terms are balanced depends on the size of the regularisation parameter λ. If λ is too small then the problem will be too close to the original ill-posed problem, but if λ is too large then the problem solved will have little connection with the original problem.

The matrix $\boldsymbol{C}$ is typically either the identity matrix $\boldsymbol{I}_m$ or a discrete approximation to a derivative operator [15]. The latter has been used in spline fitting [16] to ensure smoothness of the reconstructed data. The correct choice of $\boldsymbol{C}$ is vital to obtaining meaningful parameters $\boldsymbol{\theta}$. Varah [17] showed that a wrong choice of $\boldsymbol{C}$ can lead to

completely erroneous results. In model updating, additional information should be introduced by means of the side constraint, not present in equation (1).

In the following, the various regularisation methods (truncated SVD, generalised SVD, cross-validation, and L-curves) are described and applied to a simulated problem.

3. TRUNCATED SINGULAR VALUE DECOMPOSITION

The singular value decomposition of $\boldsymbol{A}$ [3] may be written in the form,

$$\boldsymbol{A} = \boldsymbol{U}\boldsymbol{\Sigma}\boldsymbol{V}^T, \tag{8}$$

where $\boldsymbol{U} \in \mathscr{R}^{n \times n}$ and $\boldsymbol{V} \in \mathscr{R}^{m \times m}$ are orthogonal matrices and

$$\boldsymbol{\Sigma} = diag(\sigma_1, \sigma_2, \ldots, \sigma_m) \in \mathscr{R}^{n \times m} \tag{9}$$

with

$$\sigma_1 \geqslant \sigma_2 \geqslant \cdots \geqslant \sigma_m > 0. \tag{10}$$

In ill-posed problems, two commonly occurring characteristics of the singular values have been observed [18]:

(1) The singular values σ_i, $i = 1, 2, \ldots, m$ decay steadily to zero with no particular gap in the spectrum.

(2) The left and right singular vectors $\boldsymbol{u}_i$ ($\boldsymbol{U} = [\boldsymbol{u}_1, \boldsymbol{u}_2, \ldots, \boldsymbol{u}_n]$) and $\mathbf{v}_i$ ($\boldsymbol{V} = [\mathbf{v}_1, \mathbf{v}_2, \ldots, \mathbf{v}_m]$) tend to have more sign changes in their elements as the index i increases.

Thus, when $\boldsymbol{A}$ is close to being rank deficient (with near-zero singular values) its null-space is spanned by vectors with many sign changes. From manipulation of the SVD,

$$\boldsymbol{A}\boldsymbol{\theta} = \sum_{i=1}^{m} \sigma_i \boldsymbol{u}_i (\mathbf{v}_i^T \boldsymbol{\theta}), \tag{11}$$

which shows that the high frequency components have only a small contribution to $\boldsymbol{A}\boldsymbol{\theta}$ because of the small $\sigma_i s$. However, the inverse problem of computing $\boldsymbol{\theta}$ from,

$$\boldsymbol{\theta} = \sum_{i=1}^{m} \mathbf{v}_\mathbf{i} \left(\frac{f_i}{\sigma_i}\right), \tag{12}$$

$$f_i = \boldsymbol{u}_i^{\mathrm{T}} \boldsymbol{b}, \tag{13}$$

shows that the noise effects will be amplified when $\sigma_i < f_i$.

Equation (12) provides a clue about when to truncate the singular values. If $\boldsymbol{A}$ does not contain noise then the singular values decay to zero whereas f_i decays to the noise level. The point $i = j$, where the two curves of σ_i and f_i begin a sustained deviation with increasing i, can be used as the truncation index when the noise level is unknown. This is the discrete Picard condition [17, 19] which can be interpreted as,

$$\min_{\boldsymbol{\theta}} \|\boldsymbol{\theta}\|_2 \text{ subject to: } \|\boldsymbol{A}\boldsymbol{\theta} - \boldsymbol{b}\|_2 < \sigma_j \tag{14}$$

It should be noted that the truncated SVD is incapable of taking account of the side constraint, $\boldsymbol{C}\boldsymbol{\theta} = \boldsymbol{d}$. This leads us to consider the generalised SVD.

3.1. GENERALISED SINGULAR VALUE DECOMPOSITION

In the generalised SVD [18], one considers the system of equations,

$$\left[\frac{\boldsymbol{A}}{\boldsymbol{C}}\right]\boldsymbol{\theta} = \left(\frac{\boldsymbol{b}}{\boldsymbol{d}}\right), \tag{15}$$

and obtains the decompositions of $\boldsymbol{A}$ and $\boldsymbol{C}$ in the form,

$$\boldsymbol{A} = \boldsymbol{U}\begin{bmatrix}\boldsymbol{I} & \\ & \boldsymbol{\Sigma}\end{bmatrix}\boldsymbol{X}^{-1}, \tag{16}$$

$$\boldsymbol{C} = \boldsymbol{V}[\boldsymbol{0} \quad \boldsymbol{M}]\boldsymbol{X}^{-1}, \tag{17}$$

where $\boldsymbol{X} \in \mathscr{R}^{m \times m}$ is non-singular, and the columns of $\boldsymbol{U} \in \mathscr{R}^{n \times m}$, $\boldsymbol{V} \in \mathscr{R}^{p \times p}$ are orthogonal (but not related to the matrices $\boldsymbol{U}$ and $\boldsymbol{V}$ in Section 3) and $n \geqslant m \geqslant p$. The matrices $\boldsymbol{\Sigma}$ and $\mathbf{M}$ are given by,

$$\boldsymbol{\Sigma} = diag(\sigma_1, \sigma_2, \ldots, \sigma_p), \tag{18}$$

$$1 \geqslant \sigma_1, \geqslant \sigma_2 \geqslant \cdots \geqslant \sigma_p \geqslant 0, \tag{19}$$

$$\boldsymbol{M} = diag(\mu_1, \mu_2, \ldots, \mu_p), \tag{20}$$

$$0 \leqslant \mu_1 \leqslant \mu_2 \leqslant \cdots \leqslant \mu_p \leqslant 1, \tag{21}$$

and the terms σ_i, μ_i, $i = 1, \ldots, p$, are normalised so that,

$$\sigma_i^2 + \mu_i^2 = 1. \tag{22}$$

The generalised singular values of $\begin{bmatrix}\boldsymbol{A}\\ \boldsymbol{C}\end{bmatrix}$ are then given by,

$$\gamma_i = \frac{\sigma_i}{\mu_i}, \quad i = 1, \ldots, p, \tag{23}$$

in decreasing order. The columns of $\boldsymbol{X}$ relating to the largest generalised singular values span the range of $\boldsymbol{A}$ and the null-space of $\boldsymbol{C}$. The reverse is true of the smallest generalised singular values. Morozov's complementation condition [14] states that the range of $\boldsymbol{C}$ should contain the null-space of $\boldsymbol{A}$. Therefore, the aim is to truncate the singular values at $i = j$ so that $\|\boldsymbol{A\theta} - \boldsymbol{b}\|_2 \leqslant \sigma_j$ and $\|\boldsymbol{C\theta} - \boldsymbol{d}\|_2$ is a minimum. This can be achieved by applying Picard's condition to truncate the singular values when $(\boldsymbol{u}_i^T \boldsymbol{b}\ /\sigma_i)_{i=j}$ takes a large value.

3.2. SVD—NUMERICAL EXAMPLE

The numerical example is the six-degree-of-freedom mass–spring system proposed by Kabe [20] and shown in Fig. 1. It consists of an arrangement of parallel springs so that the effects of small stiffness changes in many of the springs tend to be similar.

The parameters to be updated are the 10 stiffnesses and six masses, and the measured data consists of the first three natural frequencies and mode shapes. The latter are the normalised displacements at the six masses to which are added independent sequences of

uniformly distributed random numbers. In addition to the three-eigenvalue equations the mass–orthogonality conditions are enforced,

$$\boldsymbol{\Phi}^{\mathrm{T}}\boldsymbol{M}\boldsymbol{\Phi} = \boldsymbol{I},$$

$$\boldsymbol{\Phi}^{\mathrm{T}}\boldsymbol{K}\boldsymbol{\Phi} = \boldsymbol{\Lambda},$$

where $\boldsymbol{\Lambda}$ and $\boldsymbol{\Phi}$ are the spectral and modal matrices respectively, and $\boldsymbol{M}$ and $\boldsymbol{K}$ are the structural mass and stiffness matrices. Also, the mass terms are constrained by the total mass condition,

$$\boldsymbol{\phi}_R^T \boldsymbol{M}\boldsymbol{\phi}_R = m_{total},$$

where $\boldsymbol{\phi}_R$ is the rigid body mode.

When the eigenvalue equations are rearranged [21] so that $\boldsymbol{\theta} = (k_1, k_2, \ldots, k_{10}, m_1, m_2, \ldots, m_6)^T$ it is clear that there are 31 equations in 16 parameters (3×6 equations for each eigenvector term, 2×6 symmetric orthogonality equations; and 1 total mass equation) and the terms in $\boldsymbol{A}$ and $\boldsymbol{b}$ contain noisy data.

Side constraints are applied to set,

$$k_1 = k_5 = k_6 = k_9 = k_{10},$$

$$k_2 = k_3,$$

$$0.1\ (k_7 - k_8) = 0,$$

$$m_1 = m_4,$$

$$m_3 = m_5 = m_6.$$

The second and third constraint equations do not accurately represent the model and this is reflected in the third equation by the weight of 0.1.

Figures 2 and 3 show typical results of singular value and generalised singular value analysis for a noise level of 5% of the eigenvector terms (signal-to-noise ratio = 20). The discrete points represent the singular values, σ_i, and the ratio $(\boldsymbol{u}_i^T \boldsymbol{b}/\sigma_i)$—the discrete Picard

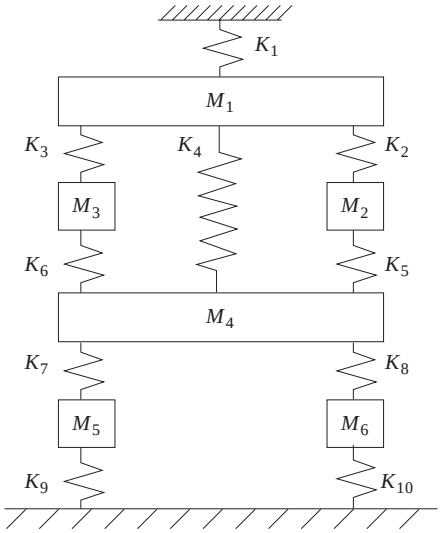

Figure 1. Numerical spring–mass model.

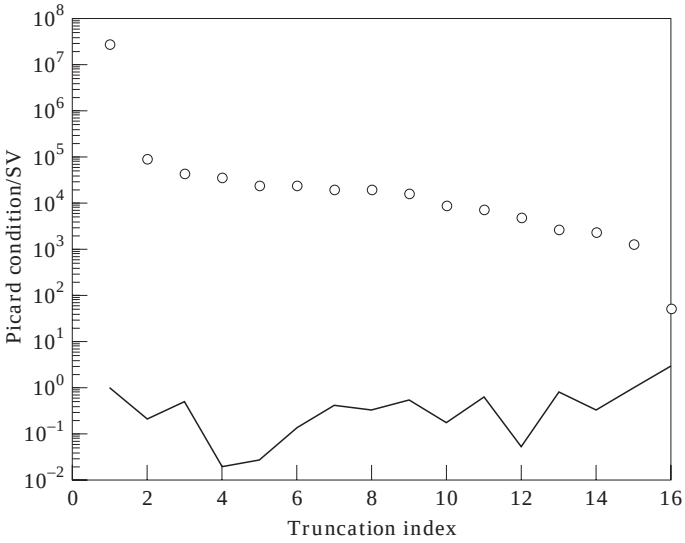

Figure 2. Singular values.

condition—is given by the sequence of points connected by straight lines. It is clear that the Picard condition fails to give a clear indication of where the singular values should be truncated.

Although the generalised SVD includes the side constraint which would be beneficial if a truncation index could be located, the Picard condition fails to find it because the level of noise in $\boldsymbol{A}$ and $\boldsymbol{b}$ is the same. This means that the σ_i and $\boldsymbol{u}_i^T \boldsymbol{b}$ decay together to the same noise level as i increases.

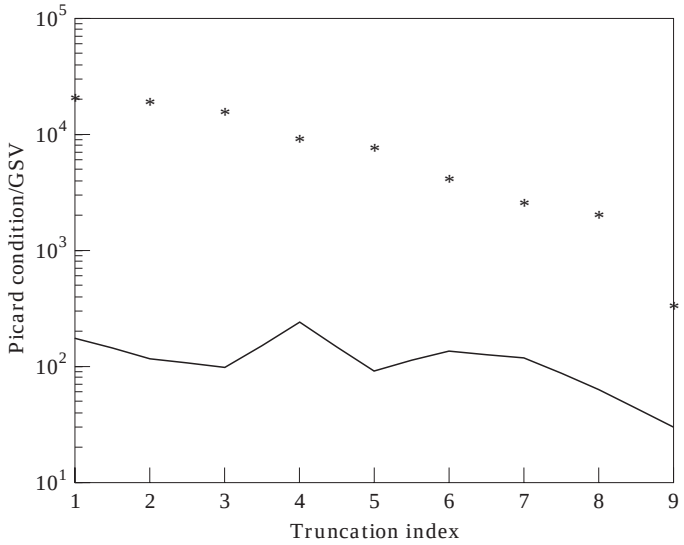

Figure 3. Generalised singular values.

4. CROSS-VALIDATION

The idea of cross-validation is to maximise the predictability of the model by choice of the regularisation parameter λ. A predictability test can be arranged by omitting one data point, b_k, $k = 1, \ldots, n$, at a time and determining an estimate, ${}_k\boldsymbol{\theta}(\lambda)$, using the other data points. Then for each of the estimates, predict the missing data and find the value of λ that on average predicts the b_k, $k = 1, \ldots, n$, best. This is the method of cross-validation [22]. The procedure is explained in the following steps.

(1) Find the estimate ${}_k\boldsymbol{\theta}(\lambda)$ which minimises,

$$\sum_{\substack{i=1 \\ i \neq k}}^{n} \left(b_i - \sum_{j=1}^{m} a_{ij}\, \theta_j \right)^2 + \lambda \| \boldsymbol{C\theta} - \boldsymbol{d} \|_2^2. \tag{24}$$

(2) Predict the missing data point,

$$\tilde{b}_k\,(\lambda) = \sum_{j=1}^{m} a_{kj}\, {}_k\theta_j\,(\lambda). \tag{25}$$

(3) Choose the value of λ which minimises the cross-validation function,

$$V_0 = \frac{1}{n} \sum_{k=1}^{n} (b_k - \tilde{b}_k\,(\lambda))^2. \tag{26}$$

From Appendix A, equation (26) may be re-written in the form,

$$V_0 = \frac{1}{n} \| \boldsymbol{Q}(\lambda)\, (\boldsymbol{A\theta}(\lambda) - \boldsymbol{b}) \|_2^2, \tag{27}$$

where

$$\boldsymbol{Q}(\lambda) = diag\left(\frac{1}{1 - r_{ii}\,(\lambda)} \right), \quad i = 1, \ldots, n, \tag{28}$$

and r_{ii} is the iith element of the influence matrix,

$$\boldsymbol{R}(\lambda) = \boldsymbol{A}(\boldsymbol{A}^T\boldsymbol{A} + \lambda \boldsymbol{C}^T\boldsymbol{C})^{-1}\boldsymbol{A}^T. \tag{29}$$

Similar expressions are derived by Craven and Wahba [23] for the case of a side constraint having the standard form $\| \boldsymbol{\theta}(\lambda) \|_2^2$. The transformation of the cost (6) to the standard form is considered by Hanke and Hansen [24], and Hansen [18] gives Matlab routines that utilise a standard-form transformation.

4.1. GENERALISED CROSS-VALIDATION

Golub *et al*. [25] showed that the 'ordinary' cross-validation method led to solutions $\boldsymbol{\theta}(\lambda)$ that were rotationally dependent. They replaced $r_{ii}\,(\lambda)$ in equation (28) with $1/n$ trace($\boldsymbol{R}(\lambda)$) to give the generalised cross-validation (GCV) function,

$$V(\lambda) = \frac{\dfrac{1}{n} \| \boldsymbol{A\theta}(\lambda) - \boldsymbol{b}) \|_2^2}{\left(\dfrac{1}{n} \text{trace}\,(\boldsymbol{I} - \boldsymbol{R}(\lambda)) \right)^2}, \tag{30}$$

which may be viewed as a weighted version of $V_0(\lambda)$. Golub *et al*. [25] showed that equation (30) could be derived from the circulant matrix which is a particular form of $\boldsymbol{D}$ that is independent of rotation.

4.2. TRUNCATION OF SINGULAR VALUES USING THE GCV

The influence matrix $\boldsymbol{R}$, given from equation (29), can be written in the form,

$$\boldsymbol{R} = \boldsymbol{A}\boldsymbol{A}^{+}, \tag{31}$$

where $\boldsymbol{A}^{+}$ denotes the generalised pseudo-inverse. In equation (28), $\boldsymbol{A}^{+}$ is a function of the regularisation parameter λ. However, the regularisation can be achieved in another way by omitting singular values. This leads us to re-write $\boldsymbol{A}^{+}$ from equation (16) in the form,

$$\boldsymbol{A}^{+} = \boldsymbol{X}\begin{bmatrix} \boldsymbol{I}_{m-p} & & \\ & \boldsymbol{\Sigma}_j^{-1} & \\ & & \boldsymbol{0}_{p-j} \end{bmatrix}\boldsymbol{U}^{T} \tag{32}$$

and,

$$\boldsymbol{A} = \boldsymbol{U}\begin{bmatrix} \boldsymbol{I}_{m-p} & & \\ & \boldsymbol{\Sigma}_j & \\ & & \boldsymbol{\Sigma}_{p-j} \end{bmatrix}\boldsymbol{X}^{-1}, \tag{33}$$

where

$$\boldsymbol{\Sigma}_j = diag(\sigma_1, \sigma_2, \ldots, \sigma_j), \tag{34}$$

$$\boldsymbol{\Sigma}_{p-j} = diag(\sigma_{j+1}, \sigma_{j+2}, \ldots, \sigma_p), \tag{35}$$

and j is the truncation index. By combining equations (31)–(33) and since $\boldsymbol{\Sigma}_j\,\boldsymbol{\Sigma}_j^{-1} = \boldsymbol{I}_j$ it is seen that,

$$\text{trace}(\boldsymbol{R}) = \text{trace}(\boldsymbol{I}_{m-p+j}) = m - p + j. \tag{36}$$

Thus,

$$\frac{1}{n}\,\text{trace}(\boldsymbol{I}_n - \boldsymbol{R}) = 1 - \frac{(m-p+j)}{n}, \tag{37}$$

and the GVC function [equation (30)] can be written as,

$$V(j) = \frac{n\,\|(\boldsymbol{A}\boldsymbol{\theta}(j) - \boldsymbol{b}\|_2^2}{(n-m+p-j)^2}. \tag{38}$$

A function similar to this (but not identical) is given by Vogel [26]. The truncation index, j, is chosen so that $V(j)$ is a minimum.

4.3. GCV—NUMERICAL RESULTS

Typical results obtained from the numerical experiment described in Section 3.2 are presented in Figs 4 and 5. The numerically produced data is identical to that described previously, with a signal-to-noise ratio of 20 as before.

The GCV function given in equation (30) is found to be sensitive to the noise and in many instances will not produce a minimum. Figure 4 illustrates one occasion when a minimum of $V(\lambda)$ was located. A problem occurs with the GCV method when the matrix $\boldsymbol{A}$ contains measured data. In the predictability test the part of the measurement noise in

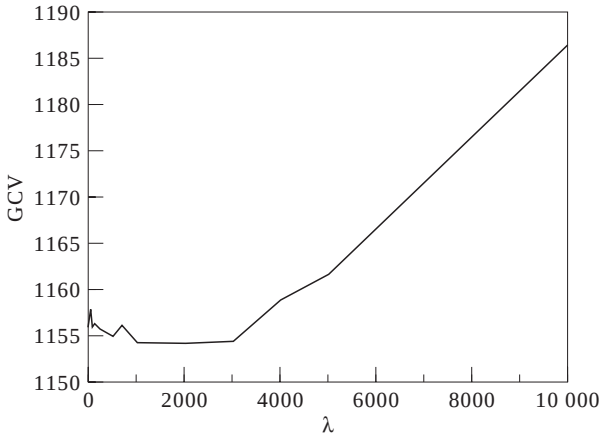

Figure 4. GCV function $V(\lambda)$.

$\boldsymbol{A}$ that is correlated with the noise in $\boldsymbol{b}$ will be regarded as the true response of the structure and only the uncorrelated part of the noise will be filtered out. In other words, the λ obtained from the GCV procedure will be smaller than the one which minimises the effect of the noise.

Figure 5 shows the GCV function $V(j)$ which is determined by truncating the generalised singular values as in equation (38). The numerical results show that $V(j)$ consistently produces a minimum at $j = 6$ and therefore seems to be more robust than $V(\lambda)$ in determining the regularisation parameter. Local minima (such as the one at $j = 2$) are noise dependent and in any case much less distinct than at $j = 6$.

5. L-CURVES

One way of obtaining a regularisation parameter in the presence of correlated noise is to define an upper bound for the side constraint and minimise the residue,

$$\min_{\boldsymbol{\theta}} \|\boldsymbol{A\theta} - \boldsymbol{b}\|_2 \quad \text{subject to: } \|\boldsymbol{C\theta} - \boldsymbol{d}\|_2 \leqslant \gamma, \tag{39}$$

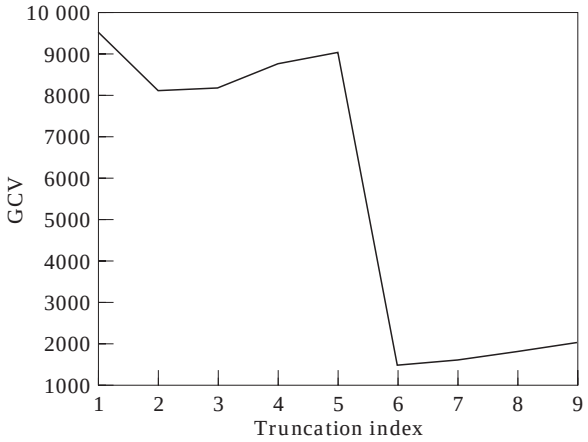

Figure 5. GCV function $V(j)$.

or alternatively to set a limit for the residue and minimise the deviation from the side constraint,

$$\min_{\boldsymbol{\theta}} \|\boldsymbol{C}\boldsymbol{\theta} - \boldsymbol{d}\|_2 \quad \text{subject to: } \|\boldsymbol{A}\boldsymbol{\theta} - \boldsymbol{b}\|_2 \leqslant \varepsilon. \tag{40}$$

Ahmadian *et al*. [27] used an equation-error method to identify the parameters of a beam from measured data by using the approach of equation (39). They used the side constraint to limit the amount of change in the initial model and assigned λ based on their judgement of allowable changes in the parameters. Of course, the success of the method is highly dependent on the physical insight of the analyst.

Another approach is to plot the norm of the side constraint $\|\boldsymbol{C}\boldsymbol{\theta}(\lambda) - \boldsymbol{d}\|_2$ against the residue $\|\boldsymbol{A}\boldsymbol{\theta}(\lambda) - \boldsymbol{b}\|_2$ obtained by minimising the cost (6) for different values of λ. Hansen [28] showed that the norm of the side constraint is a monotonically decreasing function of the norm of the residue, and any point (ε, γ) on the curve is a solution to the two constrained least-squares problems (39) and (40). He pointed out that for a reasonable signal-to-noise ratio and satisfaction of the Picard condition the curve is approximately vertical for $\lambda < \lambda_{opt}$, and soon becomes a horizontal line when $\lambda > \lambda_{opt}$, with a corner near the optimal regularisation parameter λ_{opt}. The curve is called the L-curve because of this behaviour, which can be explained as follows. When λ varies within the order of the smallest singular values of $\boldsymbol{A}$, the norm $\|\boldsymbol{A}\boldsymbol{\theta}(\lambda) - \boldsymbol{b}\|_2$ does not change significantly. However, according to Morozov's condition, the vectors (corresponding to the small singular values) occupy the range of $\boldsymbol{C}$, so that a large change is produced in $\|\boldsymbol{C}\boldsymbol{\theta}(\lambda) - \boldsymbol{d}\|_2$ which gives the vertical part of the curve. Since the small singular values contain the measurement noise it is clear that the vertical line extends further from the corner as λ becomes smaller. On the other hand, when λ increases beyond λ_{opt} the norm $\|\boldsymbol{A}\boldsymbol{\theta}(\lambda) - \boldsymbol{b}\|_2$ also tends to increase because the cost (6) then favours satisfaction of the side constraint. When the side constraint is closely satisfied then no perceptible change in $\|\boldsymbol{C}\boldsymbol{\theta}(\lambda) - \boldsymbol{d}\|_2$ is expected, and the horizontal part of the curve is created. Hansen and O'Leary [29] specify λ_{opt} as the regularisation parameter with maximum curvature at the corner of the log–log plot of the L-curve. This point represents a balance between confidence in the measurements and the analyst's intuition.

5.1. L-CURVE—NUMERICAL RESULTS

A typical L-curve for the numerical problem described previously and shown in Fig. 1 is given in Fig. 6. The curve displays a clear corner at $\lambda \approx 800$ when the signal-to-noise ratio is 20.

Identified stiffness and mass parameters are given in Table 1 by using the regularisation parameter λ (derived from L-curves) and the GSVD truncation index j (from GCV). These results are shown together with parameters obtained from an unregulated (no side constraint) least-squares solution. As expected, the unregulated least-squares estimate fails to identify an acceptable model. Negative mass and stiffness terms are found and estimation errors as high as 120% are obtained. The parameters obtained by GSVD and by the constrained least-square approach both seem to be acceptable. It is not really possible from one set of typical results to say whether the use of L-curves to determine λ, or GCV to determine j, is to be preferred. An example of regularised model updating by using data from a physical experiment is given in the following section.

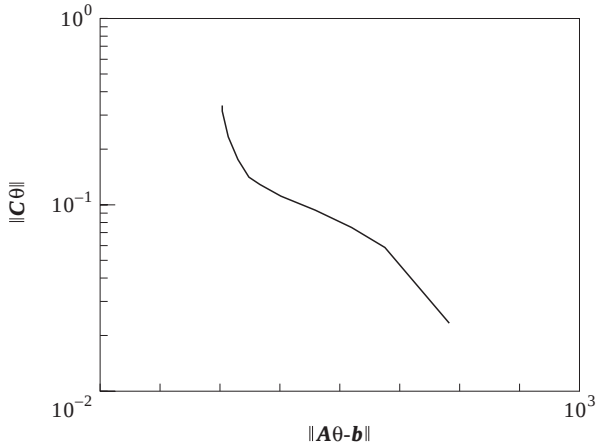

Figure 6. L-curve.

6. REGULARISED MODEL UPDATING FROM A PHYSICAL EXPERIMENT

The test structure was the frame shown in Fig. 7. It contains four L-shaped welded joints and two welded T joints which are difficult to model. The frame is made from 25.4 mm (1 inch) square aluminium tubing with 2.38 mm (3/32 inch) wall thickness. Modal analysis was performed using standard hammer-impact procedures to obtain the first five out-of-plane strain modes (natural frequencies and mode shapes measured at 13 points) from the freely suspended frame.

A finite element model consisting of 28-beam/bar elements (six-degrees-of-freedom per node) was constructed, the beam-part of each element being an Euler–Bernoulli beam

TABLE 1

Table of estimated parameters

Parameter		Signal-to-noise ratio = 100			Signal-to-noise ratio = 20		
	Exact	GSVD ($j = 7$)	CLS ($\lambda = 700$)	LS	GSVD ($j = 6$)	CLS ($\lambda = 800$)	LS
k_1	1000	957	966	1041	1348	561	954
k_2	1250	1250	1257	1266	1214	1309	1243
k_3	1500	1405	1533	1518	1008	1338	1502
k_4	10000	10098	9975	10003	9843	10358	9844
k_5	1000	984	1002	1006	1047	873	1160
k_6	1000	937	1024	1008	1155	711	1011
k_7	5000	5276	4610	9914	4062	6949	−1024
k_8	7000	6953	7896	−414	5422	12639	21382
k_9	1000	1050	932	2035	940	1197	−83
k_{10}	1000	969	1091	−63	833	1201	2323
m_1	1.0	1.005	0.992	1.0	1.0	1.033	0.97
m_2	0.2	0.2	0.201	0.2	0.2	0.194	0.21
m_3	0.1	0.093	0.102	0.1	0.101	0.077	0.1
m_4	1.0	1.0	1.0	0.99	1.026	0.939	0.95
m_5	0.1	0.107	0.094	0.2	0.09	0.118	−0.02
m_6	0.1	0.098	0.111	−0.01	0.084	0.14	0.28

GSVD, Generalised singular value decomposition; CLS, least squares with side constraint; LS, least squares without side constraint.

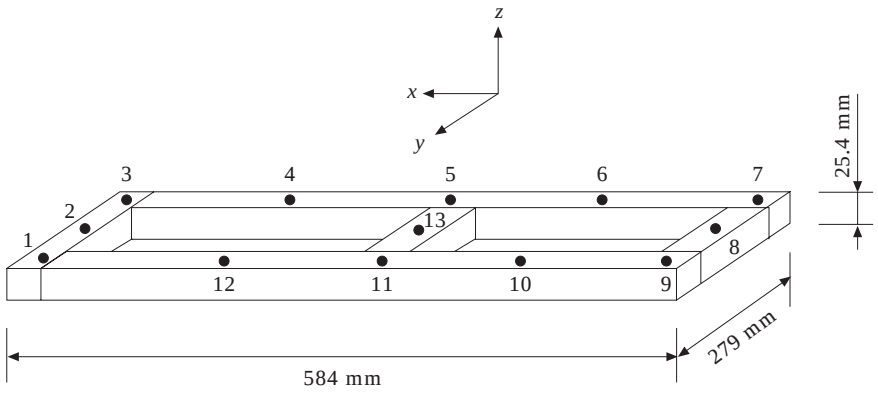

Figure 7. Frame structure.

with Hermitian shape functions. The physical properties used in the finite element model were:

Modulus of elasticity, $E = 71$ GPa;
Shear modulus, $G = 26.6$ GPa;
Mass density, $\rho = 2710\ \text{kg/m}^3$;
Area, $A = 2.19 \times 10^{-4}\ \text{m}^2$;
Principal inertia, $I = 1.3 \times 10^{-8}\ \text{m}^4$;
Torsional constant, $J = 3.91 \times 10^{-8}\ \text{m}^4$.

The joints, which were inaccurate in the finite element model, are shown in Fig. 8. Mis-modelling of the joints then represented one of the major sources of discrepancy between the finite element and test results, which are given in Table 2 and Fig. 9.

6.1. UPDATING PROCEDURE

The frame model was updated by using the generic element approach [30] which is based on the idea of adjusting the eigenvalues and mode shapes of individual elements (or groups of elements). The present case sought to correct the stiffness of the finite element model and the mass matrix was assumed to be correct. It was chosen to update the element

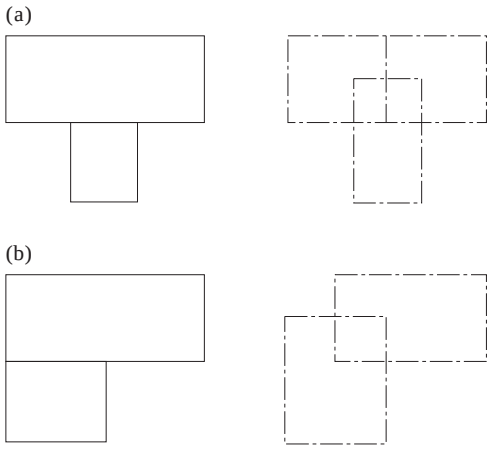

Figure 8. (a) T and (b) L joint FE models.

TABLE 2

Numerical and measured natural frequencies, frame example

	Frequency (Hz)		
Mode	F.E	Measured	Error (%)
1	255.8	226.8	12.8
2	277.5	275.2	0.9
3	581.3	537.4	8.3
4	911.3	861.5	6.0
5	1049.4	974.8	8.0

stiffnesses by adjusting the eigenvalues and eigenvectors of the element stiffness matrices. Each beam/bar element has order six and rank three and therefore decomposition of the element stiffness gives,

$$\boldsymbol{K}^e = \boldsymbol{V}_0 \boldsymbol{R}\boldsymbol{\Lambda}\boldsymbol{R}^T\boldsymbol{V}_0^T \tag{41}$$

or

$$\boldsymbol{K}^e = \boldsymbol{V}_0 \begin{bmatrix} \kappa_{11} & \kappa_{12} & \kappa_{13} \\ & \kappa_{22} & \kappa_{23} \\ \text{sym} & & \kappa_{33} \end{bmatrix} \boldsymbol{V}_0^T \tag{42}$$

where $\boldsymbol{V}_0$ contains the three strain-eigenvectors of the original finite element model, $\boldsymbol{\Lambda}$ is the diagonal matrix of stiffness eigenvalues, $\boldsymbol{R}$ is the 3×3 rotation matrix given from,

$$\boldsymbol{V} = \boldsymbol{V}_0 \boldsymbol{R} \tag{43}$$

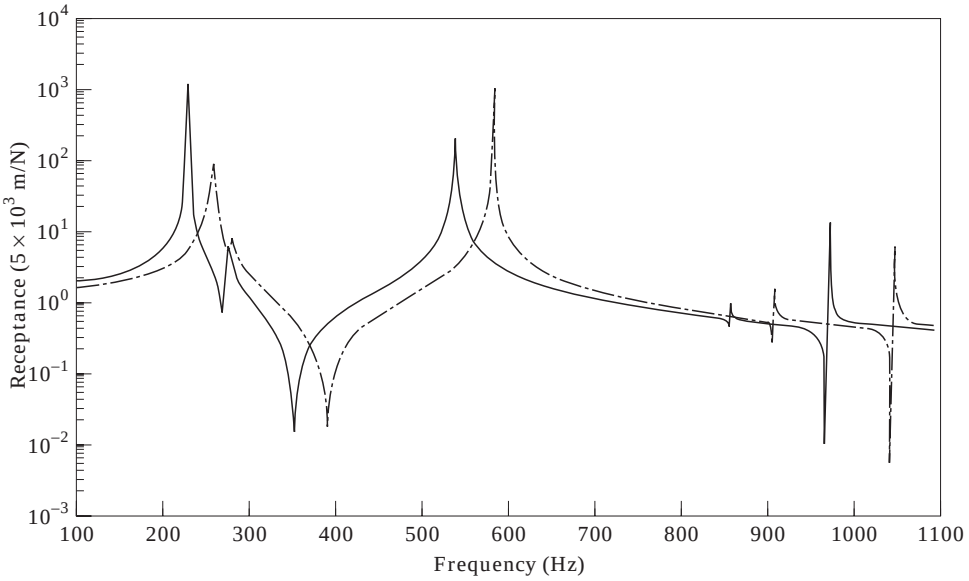

Figure 9. Measured (——) and finite element (– · – · –) frequency responses.

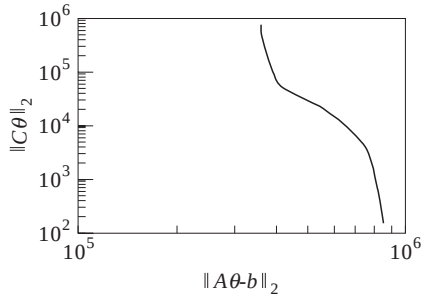

Figure 10. L-curve—frame example.

and $\boldsymbol{V}$ is the matrix of corrected element stiffness eigenvectors. The terms $\kappa_{11}, \ldots, \kappa_{33}$ are open for updating. For the beam/bar element it can be shown that,

$$\boldsymbol{V}_0^T = \begin{bmatrix} 0 & \alpha & 0 & 0 & -\alpha & 0 \\ 2\beta & \beta & 0 & -2\beta & \beta & 0 \\ 0 & 0 & \alpha & 0 & 0 & -\alpha \end{bmatrix} \tag{44}$$

where $\alpha = \sqrt{2}/2$ and $\beta = \sqrt{10}/10$. Thus, the first and third modes are anti-symmetric and the second mode is symmetric. Thus, for any symmetric beam/bar element κ_{12} and κ_{23} are zero. Then for each of the 14-joint elements, there are six correction parameters, and four correction parameters at each of the connecting elements, making 140 parameters in total to be updated. These parameters are determined from the 70 equations arising from the five measured modes and a further 340 equations obtained from expanding the mode shapes using the finite element model [31]. To constrain the solution it is assumed that similar elements are given by a similar model. Based on their similarities, the elements can be grouped into three sets: T joint elements, L joint elements, and connecting elements. This grouping of the elements constitutes the side constraint.

6.3. RESULTS

The L-curve for the frame problem has a clear corner as shown in Fig. 10. The reconstructed frequencies are given in Table 3, together with results that had been produced by using a minimum-norm constraint. Both methods give reconstructed frequencies that are in excellent agreement with the measured data. However, a stricter

TABLE 3

Reconstructed natural frequencies, frame example

	Frequency (Hz)		
Mode	Measured	Element groups constraint	Minimum norm.
1	226.8	226.9	226.8
2	275.2	275.1	275.0
3	537.4	537.4	537.4
4	861.5	861.5	861.5
5	974.8	974.8	974.8
6	—	1255.6	1251.2
7	—	1521.4	1520.3

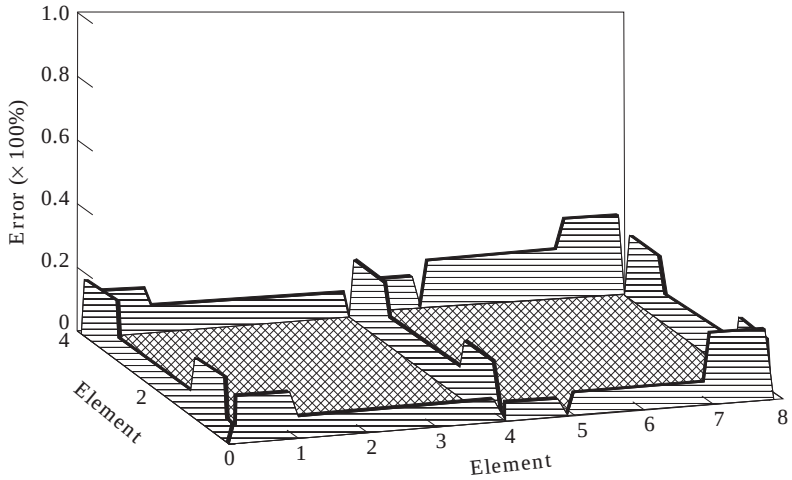

Figure 11. Adjustment of stiffnesses—element groups constraint.

test is that the updated parameters should provide physical understanding. In Figs 11 and 12, the stiffness adjustment, $\|\Delta \boldsymbol{K}_i^e\|_2 / \|\boldsymbol{K}_{0i}^e\|_2$, is superimposed on the frame arrangement. It can be seen that the minimum norm solution leads to parameters which do not seem to be adjusted in any sensible way. The grouped-elements side constraint, on the other hand, shows that the parameters which received the most correction were at the joints, as would be expected. It is clear that the grouped-element constraint is preferable; it has smaller changes than the minimum-norm solution, and the corner of the L-curve appears to have resulted in a solution with physical understanding.

7. CONCLUSIONS

The importance of selecting a good side constraint has been demonstrated. The regularisation parameter can be determined by a number of methods, but the present study has indicated that the GCV method for truncating generalised singular values, and the

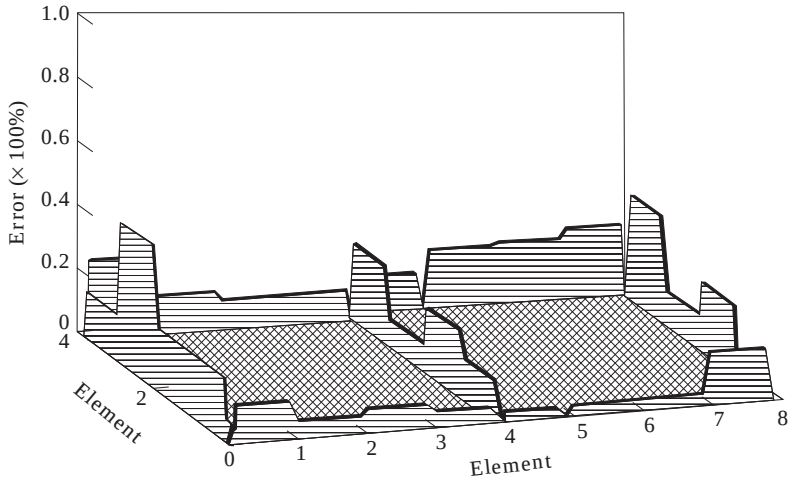

Figure 12. Adjustment of stiffnesses—minimum norm constraint.

L-curves method, are robust in the presence of noise, and provide reliable results. A finite element model was updated with physical test data by using a regularisation parameter determined from an L-curve.

ACKNOWLEDGEMENTS

Dr Friswell gratefully acknowledges the support of the Engineering and Physical Sciences Research Council through the award of an Advanced Fellowship.

REFERENCES

1. J. E. Mottershead and M. I. Friswell 1993 *Journal of Sound and Vibration* **167**, 347–375. Model updating in structural dynamics: a survey.
2. M. I. Friswell and J. E. Mottershead 1995 *Finite Element Model Updating in Structural Dynamics*. Dordrecht: Kluwer.
3. G. H. Golub and C. F. Van Loan 1989 *Matrix Computations*, 2nd edn. Baltimore: John Hopkins Univ. Press.
4. I. U. Ojalvo and T. Ting 1990 *AIAA Journal* **28**, 1976–1979. Interpretation and improved solution approach for ill-conditioned linear equations.
5. L. Zhang and I. U. Ojalvo 1992 *Proceedings of the 10th IMAC*, 591–594. An improved epsilon decomposition approach for structural system identification.
6. J. E. Mottershead and C. D. Foster 1991 *Mechanical Systems and Signal Processing* **5**, 139–154. On the treatment of ill-conditioning in spatial parameter estimation from measured vibration data.
7. E. Rothwell and B. Drachman 1989 *International Journal of Numerical Methods in Engineering* **28**, 609–620. A unified approach to solving ill-conditioned matrix problems.
8. H. G. Natke 1992 *Proceedings of the 9th IMAC*, 70–73. On regularisation methods applied to the error localisation of mathematical models.
9. H. G. Natke 1992 *IUTAM Symposium on Inverse Problems in Engineering Mechanics*, **3–20,** 11–15 *May*, *Tokyo*. Regularisation methods within system identification.
10. A. Fregolent, W. D'Ambrogio, P. Salvini and A. Sestieri 1996 *Inverse Problems in Engineering* **2**, 171–200. Regularisation techniques for dynamic model updating using input residual.
11. M. Link 1993 *Proceedings of Modern Practice in Stress and Vibration Analysis*, 35–52. Updating of analytical models—Procedures and Experience.
12. U. Prells 1996 *Inverse Problems in Engineering*, **3**, 197–217. A regularisation method for the linear error localisation of models of elastomechanical systems.
13. A. N. Tikhonov and V. Y. Arsenin 1977 *Solutions of Ill-Posed Problems*. New York: John Wiley.
14. V. A. Morozov 1984 *Methods for Solving Incorrectly Posed Problems*. New York: Spring-Verlag.
15. L. D. Phillips 1962 *Journal of the Association of Computational Machining* **9**, 84–97. A technique for the numerical solution of certain integral equations of the first kind.
16. G. Wahba 1990 *Spline Models for Observational Data*. Philadelphia: SIAM.
17. J. M. Varah 1983 *SIAM Journal of Scientific and Statistical Computation* **4**, 164–176. Pitfalls in solution of linear ill-posed problems.
18. P. C. Hansen 1994 *Numerical Algorithms* **6**, 1–35. Regularisation tools: a MATLAB package for analysis and solution of discrete ill-posed problems.
19. P. C. Hansen 1990 *BIT* **30**, 658–672. The discrete Picard condition for discrete ill-posed problems.
20. A. M. Kabe 1985 *AIAA Journal* **23**, 1431–1436. Stiffness matrix adjustment using mode data.
21. J. C. O'Callahan and C. H. Wu 1991 *Proceedings of the 9th IMAC*, 580–590. System identification and localisation procedures with structural connectivity constraint.
22. M. Stone 1974 *Royal Statistics Society* **36**, 111–147. Cross-validatory choice and assessment of statistical prediction.
23. P. Craven and G. Wahba 1979 *Numerische Mathematik* **32**, 377–403. Smoothing noisy data with spline functions.

24. M. HANKE and P. C. HANSEN 1993 *Surveys on Mathematics for Industry* **3**, 253–315. Regularisation methods for large-scale problems.
25. G. H. GOLUB, M. HEATH and G. WAHBA 1979 *Technometrics* **21**, 215–223. Generalised cross-validation as a method for choosing a good ridge parameter.
26. C. R. VOGEL 1986 *SIAM Journal of Numerical Analysis*, **23**, 109–117. Optimal choice of a truncation level for the truncated SVD solution of linear first kind integral equations when data are noisy.
27. H. AHMADIAN, G. M. L. GLADWELL and F. ISMAIL *Journal of Sound and Vibration* **172**(Suppl.), 657–699. Finite element model identification using model data.
28. P. C. HANSEN 1992 *SIAM Review* **34**, 561–580. Analysis of discrete ill-posed problems by means of the L-curve.
29. P. C. HANSEN and D. P. O'LEARY 1993 *SIAM Journal of Scientific Computation* **14**, 1487–1503. The use of the L-curve in the regularisation of discrete ill-posed problems.
30. G. M. L. GLADWELL and H. AHMADIAN 1995 *Mechanical Systems and Signal Processing* **9**, 601–614. Generic element matrices suitable for finite element model updating.
31. H. AHMADIAN, G. M. L. GLADWELL and F. ISMAIL *ASME Journal of Vibration and Acoustics* **119**, 37–45. Parameter selection strategies in finite element model updating.

APPENDIX A: CROSS VALIDATION FUNCTION

Equation (26) gives the cross-validation function as,

$$V_0 = \frac{1}{n}\sum_{k=1}^{n}(b_k - \tilde{b}_k(\lambda))^2. \tag{A1}$$

To simplify the CV function consider the identity,

$$b_k - \tilde{b}_k = \frac{b_k - \sum_{j=1}^{m} a_{kj}\,\theta_j(\lambda)}{1 - \tilde{r}_{kk}}, \tag{A2}$$

where,

$$\tilde{r}_{kk} = \frac{\sum_{j=1}^{m} a_{kj}\,\theta_j(\lambda) - \tilde{b}_k}{b_k - \tilde{b}_k}, \tag{A3}$$

and $\theta_j(\lambda)$ is the jth term in $\boldsymbol{\theta}(\lambda)$. Since $\tilde{b}_k = \sum_{j=1}^{m} a_{kj\ k}\theta_j(\lambda)$ it follows that,

$$\tilde{r}_{kk} = \sum_{j=1}^{m} \frac{a_{jk}\,(\theta_j(\lambda) - {}_k\theta_j(\lambda))}{b_k - \tilde{b}_k}. \tag{A4}$$

Replacing the divided difference by a derivative it is found that,

$$\tilde{r}_{kk} = \frac{\partial}{\partial \boldsymbol{b}_k}\left(\sum_{j=1}^{m} a_{kj}\,\theta_j(\lambda)\right) = r_{kk}(\lambda), \tag{A5}$$

where r_{kk} is the kkth entry of the influence matrix given in equation (29). Combining equations (A1), (A2) and (A5) gives,

$$V_0(\lambda) = \frac{1}{n}\sum_{k=1}^{n}\left[\frac{b_k - \sum_{j=1}^{m} a_{kj}\,\theta_j(\lambda)}{1 - r_{kk}}\right]^2, \tag{A6}$$

which is identical to equation (27).